2014 IEEE International Conference on Robotics & Automation (ICRA)
Hong Kong Convention and Exhibition Center
May 31 - June 7, 2014. Hong Kong, China

Exploiting the Dynamics of a Robotic Manipulator for Control of UAVs

Abeje Y. Mersha, Stefano Stramigioli, and Raffaella Carloni

***Abstract*— This paper presents a new free-flight controller for aerial manipulators, unmanned aerial vehicles endowed with a robotic manipulator. The control strategy exploits the dynamics of the manipulator to improve the tracking performance and maneuverability of the UAV by expanding its flight envelop. The controller increases the spectrum of deployable manipulators, which otherwise are limited to be light-weighted manipulators and with a dynamics that do not significantly affect the UAV. The effectiveness and applicability of the proposed controller is verified through simulations and experiments.**

I. Introduction

Recent research in the field of aerial robotics focuses on developing manipulation systems in order to perform task specific aerial interactions. Aerial inspection by contact [1], aerial grasping [2], [3], load transportation and cooperative aerial assembling [4] are some of the resounding research achievements in the field of aerial interaction.

Unmanned aerial vehicles (UAVs), endowed with robotic manipulators and hereafter referred as aerial manipulators, have been employed for most of the aforementioned applications. The appended manipulators are often designed to be light-weighted [5], [6], and are commonly placed as close to the center of mass (COM) of the UAV as possible [2], [5]. The primary motivations for such design and placement choices are to avoid significant change in the inertia property of the UAV and/or to minimize the influence of the dynamics of the manipulator and the gravitational bias torque due to the manipulator. As such, existing classical UAV controllers can still be used without major modification.

Generally, the UAV controllers of such aerial manipulators, as yet, are variants of classical PID controllers [2], [5], [7]. These controller attempt to reject disturbances, including those due to the dynamics of the manipulator. Commonly, during free-flight, the movement of the manipulator is constrained [1], [6], and the static shift of COM and change in the rotational inertia of the aerial manipulator are possibly compensated by the integral action of the UAV's PID controller. Some works even suggested to compensate for the shift in the position of the COM by placing a counterbalancing mass on the opposite side of the UAV [6], which even increases the overall mass and rotational inertia of the complete system. These approaches certainly limit the class of deployable manipulators to those with certain mechanical configuration and dynamics. Moreover, the use of classical UAV controllers results in poor tracking performance, and even sometimes lead to stability issues.

The main contribution of this paper is a free-flight control architecture for aerial manipulators based on the unified dynamics of the UAV and the manipulator. The architecture exploits the dynamic disturbance of the manipulator on the UAV to improve the trajectory tracking performances of the underactuated UAV. The advantage of the proposed controller over classical PID controllers is twofold. First, better tracking performance and robustness can be achieved. Second, it exploits the dynamics of a manipulator to achieve a better maneuverability of the UAV by extending the flight-envelop. The advantages of the proposed controller are corroborated by simulations and experimental results on a quadrotor UAV.

II. Dynamics of an Aerial Manipulator

Inspired by the ubiquity of quadrotors as research platforms, this section provides the kinematics and dynamics of a planar quadrotor UAV on which a 1D manipulator with a prismatic joint is mounted. The motivation behind using the simplified planar dynamics is to provide easy and intuitive insights about its dynamics and the proposed controller. Besides, it limits the mathematical complexity while still capturing the main features of its 3D counterpart, which is used for experimental verification.

With respect to Fig. 1 that shows the planar aerial manipulator, the following are defined:

- $\psi^0 = [o_0, \overrightarrow{\hat{x}_0}, \overrightarrow{\hat{y}_0}]$ and $\psi^u = [o_u, \overrightarrow{\hat{x}_u}, \overrightarrow{\hat{y}_u}]$ denote the planar inertial coordinate frame and the body-fixed coordinate frame attached to the COM of the UAV.
- $c \in \mathbb{R}^+$ is a nonzero constant lateral displacement of each propeller from ψ^u.
- $h \in \mathbb{R}^+$ is a constant vertical displacement of the COM of the manipulator from ψ^u.
- $\ell \in \mathbb{R}$ is a lateral displacement of the COM of the manipulator from ψ^u.
- $R_u^0 \in \mathbb{R}^{2\times 2}$ is the orthonormal rotational matrix describing the orientation of ψ^0 with respect to ψ^u, and it transforms coordinates from ψ^u to ψ^0.
- m and I denote the mass and the inertia of the manipulator (subscript m) and of the UAV (subscript u).
- F_{ug} and F_{mg} represent the gravitational forces of the UAV and the manipulator, respectively.
- F_1, F_2 and F_3 represent the actuation forces of the two propellers and of the manipulator.

Moreover, for generic vectors and matrix x, x_a and M:

This research is supported by the European Commission's 7^{th} Framework Program as a part of the project "Innovative Aerial Service Robots for Remote Inspection by Contact (AIRobots)" under grant number 248669 and "Smart collaboration between humans and ground-aerial robots for improving rescuing activities in alpine environments (SHERPA)" under grant number 600958.

The authors are with the Faculty of Electrical Engineering, Mathematics and Computer Science, Robotics and Mechatronics group, CTIT institute, University of Twente, The Netherlands. Email: {a.y.mersha, s.stramigioli, r.carloni}@utwente.nl

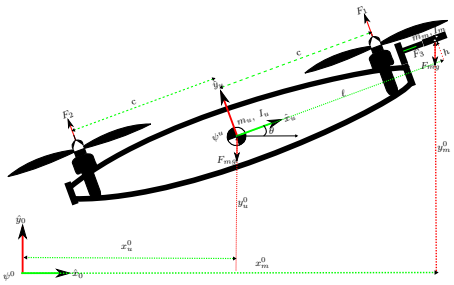

Fig. 1. Planar aerial manipulator consisting of a planar quadrotor on which a 1D robotic manipulator with a prismatic joint is appended.

- x_i (or x_{a_i}) indicates the i^{th} entry of vector x (or x_a) .
- m_{ij} indicates the i^{th} row and j^{th} column entry of the matrix M.
- $M_{ij,kl}$ (or $M^{-1}_{ij,kl}$) indicates a sub-matrix of M (or M^{-1}) that contains entries of $i^{th}-j^{th}$ row and $k^{th}-l^{th}$ column.

For scalars:

- κ^i_j denotes the $\kappa \in \{\theta,\ x,\ y\}$ (rotational, lateral or vertical) coordinates of the generalized configuration of $j \in \{m,\ u\}$ (manipulator or UAV) with respect to $i \in \{0,\ u\}$ (ψ^0 or ψ^u).
- $\dot{\kappa}^{k,i}_j$ denotes the $\kappa \in \{\theta,\ x,\ y\}$ component of the generalized velocity of $j \in \{m,\ u\}$ with respect to $i \in \{0,\ u\}$ in coordinates of $k \in \{0,\ u\}$.

Let $p^0_u := \begin{bmatrix} x^0_u & y^0_u \end{bmatrix}^T$ and $p^u_m := \begin{bmatrix} x^u_m & y^u_m \end{bmatrix}^T = \begin{bmatrix} \ell & h \end{bmatrix}^T$, the geometric relation of the generalized planar configuration of the aerial manipulator is

$$\begin{cases} \theta_m = \theta_u = \theta \\ p^0_m = p^0_u + R^0_u p^u_m \end{cases} \tag{1}$$

and, therefore, the velocity relation is given by

$$\begin{cases} \omega^{m,0}_m &= \omega^{u,0}_u = \dot{\theta} \\ \dot{p}^0_m &= \dot{p}^{0,0}_u + R^0_u \dot{p}^{u,u}_m + \dot{R}^0_u p^u_m \\ &= \dot{p}^0_u + \dot{\ell} R^0_u \begin{bmatrix} 1 \\ 0 \end{bmatrix} + \omega^{u,0}_u R^0_u S(1) p^u_m \end{cases} \tag{2}$$

where $S(1) = \begin{bmatrix} 0 & -1 \\ 1 & 0 \end{bmatrix}$ is a skew symmetric matrix.

A unified dynamics of the complete system is derived by using the Newton-Euler approach. The considered benchmark is composed of two planar rigid bodies (the manipulator and the UAV, each with 3DOFs) that are connected by a 1D prismatic joint. Due to this joint, the complete aerial manipulator has only 4DOFs. The first three equations describing the closed form of the dynamics of the aerial manipulator are obtained by eliminating the generalized internal forces between the two subsystems, i.e.,

$$m_u \ddot{p}^{0,0}_u + m_m \ddot{p}^{0,0}_m = R^0_u \begin{bmatrix} 0 \\ F_1 + F_2 \end{bmatrix} + \begin{bmatrix} 0 \\ F_{ug} + F_{mg} \end{bmatrix} \tag{3}$$

$$\begin{cases} (I_u + I_m)\dot{\omega}^{u,\ 0}_u + m_m (S(1)p^u_m)^T R^u_0 \ddot{p}^{0,0}_m = c(F_1 - F_2) + \\ (p^u_m)^T R^u_0 \begin{bmatrix} 0 \\ F_{mg} \end{bmatrix} \end{cases} \tag{4}$$

The dynamics of the fourth DOF can be obtained by resolving the translational motion of the manipulator with respect to ψ^0 along its line of motion, i.e., along $\overrightarrow{\hat{x}_u}$,

$$m_m \begin{bmatrix} 1 & 0 \end{bmatrix} R^u_0 \ddot{p}^{0,0}_m = F_3 + \begin{bmatrix} 1 & 0 \end{bmatrix} R^u_0 \begin{bmatrix} 0 \\ F_{mg} \end{bmatrix} \tag{5}$$

For brevity, the complete dynamics given in (3) - (5) with the addition of viscous damping is compactly represented by

$$M(x_1)\dot{x}_2 + C(x_1, x_2)x_2 + Dx_2 + G(x_1) = B(x_1)u \tag{6}$$

where $x^T_1 := \begin{bmatrix} x^0_u & y^0_u & \theta & \ell \end{bmatrix}$ and $x_2 := \dot{x}_1$; the control input $u^T := \begin{bmatrix} F_1 & F_2 & F_3 \end{bmatrix}$; $M(x_1)$, $C(x_1, x_2)$, D and $B(x_1)$ denote the generalized mass, centrifugal and coriolis, damping, and input matrices, respectively; $G(x_1)$ denotes the gravitational force vector. The entries of these matrices and vector are given in the Appendix.

III. Controller Design

In this section, the proposed nonlinear controller design is presented. As depicted in Fig. 2, the controller relies on output feedback linearization and stable zero dynamics. To facilitate the control design, the standard state space representation of the dynamics of the planar aerial manipulator is used.

Let the states of the aerial manipulator be $x^T := \begin{bmatrix} x^T_1 & x^T_2 \end{bmatrix} \in \mathbb{R}^8$, the state space representation of its dynamics given by (6) is

$$\begin{cases} \overbrace{\begin{bmatrix} \dot{x}_1 \\ \dot{x}_2 \end{bmatrix}}^{\dot{x}} = \overbrace{\begin{bmatrix} x_2 \\ -\ M^{-1}(x_1)\{C(x_1, x_2)x_2 + Dx_2 + G(x_1)\} \end{bmatrix}}^{f(x)} \\ \qquad + \overbrace{\begin{bmatrix} 0 \\ M^{-1}(x_1)B(x_1) \end{bmatrix}}^{g(x)} u \\ y \ = \ h(x) = \begin{bmatrix} x^0_u & y^0_u & \ell \end{bmatrix}^T \end{cases} \tag{7}$$

where $f(x)$ and $g(x)$ are the drift and input vector fields, respectively; $h(x)$ is a vector of smooth functions; $u, y \in \mathbb{R}^3$ are the input and output vectors of the system.

A. Feedback Linearization

The dynamics of the aerial manipulator described by (7) is flat with respect to the flat output vector y, implying that the system is dynamic feedback linearizable, [8], [9]. However, it is not static feedback linearizable with respect to y, [10]. Nonetheless, static feedback linearization based on cascaded control strategy, [11], [12], is chosen over dynamic feedback linearization to reduce the complexity. With the aim of controlling y, an intermediate output vector $z^T = \begin{bmatrix} y^0_u & \theta & \ell \end{bmatrix}$ is defined. With respect to z, the aerial manipulator has the following properties:

1) It has a relative degree vector $r = \begin{bmatrix} r_1 & r_2 & r_3 \end{bmatrix}$, where $L_{g_j} L^k_f h_i(x) = 0,\ \forall j \mid 1 \le j \le 3,\ \forall k \mid k < r_i - 1,\ \forall i \mid 1 \le i \le 3$, in which L is the Lie derivative. For the aerial manipulator, $r_i = 2$.

2) The 3×3 matrix given by

$$\alpha(x) = \begin{pmatrix} L_{g_1}L_f h_1(x) & L_{g_2}L_f h_1(x) & L_{g_3}L_f h_1(x) \\ L_{g_1}L_f h_2(x) & L_{g_2}L_f h_2(x) & L_{g_3}L_f h_2(x) \\ L_{g_1}L_f h_3(x) & L_{g_2}L_f h_3(x) & L_{g_3}L_f h_3(x) \end{pmatrix}$$

has a rank $(\alpha(x)) = 3$, $\forall x \in \mathbb{R}^8 | \{c = 0\}$, where c is the lateral displacement of the propellers (see, Fig. 1). Since $c \neq 0$, $\alpha(x)$ is always invertible.

Based on the above properties, (7) is input-output linearizable with $u = \alpha^{-1}(x_1)\{-\beta(x_1, x_2) + v\}$, where $\beta(x_1, x_2) = -M_{24,14}^{-1}(x_1)\{C(x_1, x_2)x_2 + Dx_2 + G(x)\}$, and $v \in \mathbb{R}^3$ is a new input vector to the feedback linearized system. However, since the dimension of the state is 8 and its total relative degree is 6, there are two states whose dynamics belong to the internal dynamics of the system. The zero dynamics of the system is

$$\begin{cases} \dot{x}_{1_1} = x_{2_1} \\ \dot{x}_{2_1} = -\frac{d_x}{m_u + m_m} x_{2_1} \end{cases} \tag{8}$$

Clearly, (8) is a linear system, whose eigenvalues are $\lambda_1 = -\frac{d_x}{m_u+m_m}$ and $\lambda_2 = 0$. Thus, the zero dynamics of the planar aerial manipulator is stable.

B. State Feedback and Feed-forward Controller

After feedback linearization, (7) reduces to

$$\begin{bmatrix} \dot{x}_1 \\ \dot{x}_{2_1} \\ \dot{x}_{2_{2,4}} \end{bmatrix} = \begin{bmatrix} x_2 \\ \varrho(x_1, x_2, v) \\ v \end{bmatrix} \tag{9}$$

where $\varrho(x_1, x_2, v)$ is a function that represents the lateral dynamics after feedback linearization (see the Appendix).

To achieve a good tracking performance, a combination of state feedback and feed-forward controller can be designed for the decoupled linear dynamics of the last three DOFs of the system, i.e., $\begin{bmatrix} y_u^0 & \theta & \ell \end{bmatrix}$. The control input to the feedback linearized system is

$$v = \dot{\bar{x}}_{2_{2,4}} + K_d(\bar{x}_{2_{2,4}} - x_{2_{2,4}}) + K_p(\bar{x}_{1_{2,4}} - x_{1_{2,4}}) \tag{10}$$

$K_p = \text{diag}(k_{py}, k_{p\theta}, k_{p\ell})$, $K_d = \text{diag}(k_{dy}, k_{d\theta}, k_{d\ell}) \in \mathbb{R}^{3\times3}$ are positive definite diagonal matrices representing the proportion and derivative gains of the feedback controller; the bar indicates the desired reference of the respective states.

Because of the underactuation of the system, the lateral dynamics in the present form can not be controlled directly. However, control of the lateral position is of primary importance in most free-flights. To address this problem, $\bar{x}_{1_3}$ is generated in such a way that the desired lateral trajectory is tracked. Under a reasonable assumption that the manipulator and pitch dynamics are time scale separated from the lateral dynamics, it follows that $\dot{x}_{2_1} \cong \varrho(x_1, x_2, v_1)$ (see the Appendix). Now, $\varrho(x_1, x_2, v_1)$ can be considered as a virtual input to the lateral dynamics. To track a lateral reference trajectory, the desired virtual input $\bar{\varrho}(x_1, x_2, v_1)$ can be designed as

$$\bar{\varrho}(x_1, x_2, v_1) = \dot{\bar{x}}_{2_1} + k_d(\bar{x}_{2_1} - x_{2_1}) + k_p(\bar{x}_{1_1} - x_{1_1}) \tag{11}$$

$\bar{x}_{1_3}$ can be uniquely extracted from the (9) and (11) with additional constraints on $\|\bar{x}_{1_3}\|_\infty < \frac{\pi}{2}$ and $\underline{v}_1 > g$.

To increase the robustness of the designed controller against measurement error, parametric uncertainties and static disturbances, saturated integral control action can be introduced in the control laws given in (10) and (11).

C. Manipulator Trajectory Planning

It is clear from (9) that the manipulator's position ($x_{1_4} = \ell$) can be independently controlled. But from task viewpoint, free-flight in this case, the main DOFs are the vertical and lateral dynamics. Thus, ℓ, which is usually constrained during free-flight, can be exploited for secondary tasks.

In this work, the manipulator is exploited to achieve a better maneuverability by expanding the flight envelope of the aerial manipulator with respect to its constrained counterpart. Since the pitch dynamics is crucial for control of the overall system, due to the underactuation, the manipulator's path is generated based on the desired pitch acceleration ($\dot{\bar{x}}_{2_3} = \ddot{\theta}_d$).

The path is generated to move the COM of the robotic manipulator in order to influence the pitch dynamics by

- changing the rotational inertia of the complete system
- modifying the influence of gravitational torque
- exploiting the toque due to the actuator force on the prismatic joint

A 5^{th} order polynomial function is used to generate a smooth trajectory up to its second derivative, fulfilling 6 constraints, $\bar{x}_{1_4}(t_i) = x_{1_4}(t_i)$, $\bar{x}_{2_4}(t_i) = x_{2_4}(t_i)$, $\dot{\bar{x}}_{2_4}(t_i) = \dot{x}_{2_4}(t_i)$ and $\bar{x}_{1_4}(t_f) = \ell \in [\underline{\ell}, \bar{\ell}]$, $\bar{x}_{2_4}(t_f) = 0$, $\dot{\bar{x}}_{2_4}(t_f) = 0$; where t_i and t_f denote the initial and final time, respectively.

Let $a^T := \begin{bmatrix} a_5 & a_4 & a_3 & a_2 & a_1 & a_0 \end{bmatrix}$ and $\zeta^T := \begin{bmatrix} \bar{x}_{1_4}(t_i) & \bar{x}_{1_4}(t_f) & \bar{x}_{2_4}(t_i) & \bar{x}_{1_4}(t_f) & \dot{\bar{x}}_{2_4}(t_i) & \dot{\bar{x}}_{2_4}(t_f) \end{bmatrix}$, then the coefficients of the polynomial function a_i, for $i = 1, 2, 3, 4, 5$, can be computed as $a = \delta(t_i, t_f)\ \zeta$, where $\delta \in \mathbb{R}^{6\times6}$ is the manipulator path planning function.

In the path generation, $t_f = t_i + \Delta$, where Δ is a variable through which the rate of change of the path is related to $\dot{\bar{x}}_{2_3}$. In this work, Δ is selected from set of possible values that are inversely proportional to $\dot{\bar{x}}_{2_3}$, i.e., the higher the desired pitch acceleration, the faster the desired change in the position of the COM of the manipulator becomes.

IV. Stability Analysis

The stability of the aerial manipulator with the proposed controller can be shown in two steps. First, the stability of the two subsystems (the feedback linearizable and the internal dynamics) is shown independently. Then, the stability of their interconnection dynamics is presented.

A. Stability of the Feedback Linearizable Dynamics

As shown in Sec. III-A, the feedback linearizable dynamics of the aerial manipulator are the y_u^0, θ and ℓ dynamics. Using the intermediate output z, we define the error vector $e_1 := \bar{z} - z$, and its rate $e_2 := \dot{e}_1$. With reference to (9) and (10), the error dynamics of the controlled linearizable part of the system is then given by

$$\begin{pmatrix} \dot{e}_1 \\ \dot{e}_2 \end{pmatrix} = \begin{pmatrix} 0_{3\times3} & I_{3\times3} \\ -K_p & -K_d \end{pmatrix} \begin{pmatrix} e_1 \\ e_2 \end{pmatrix} \tag{12}$$

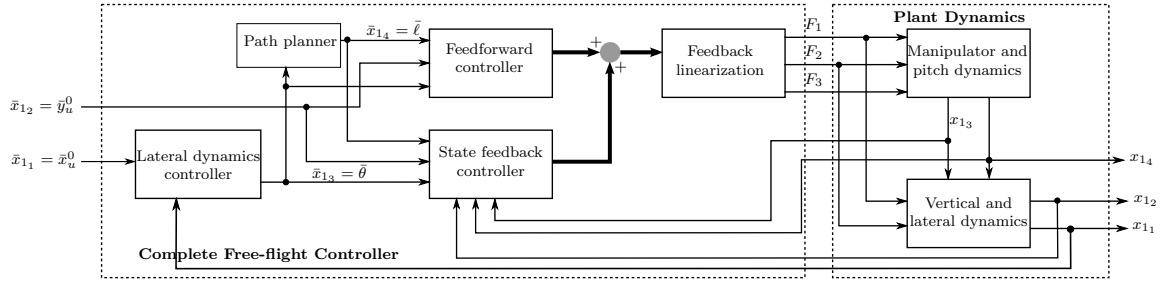

Fig. 2. The proposed free-flight controller that is based on the unified dynamics of the aerial manipulator that exploits the dynamics of the robotic manipulator mounted on it. The labeled signals also represent their first and second time derivatives.

where $I_{3\times3}$ and $0_{3\times3}$ are 3×3 identity and zero matrices.

Proposition 1: *The control input of the system u given in Sec. III-A, in which the intermediate control input v is defined by (10), exponentially stabilizes the vertical, rotational and manipulator dynamics of the aerial manipulator.*

Proof: Direct substitution of u and v in (eq:ARStateSpace) results in an error dynamics given in (12), whose system matrix is Hurwitzian as long as K_p and K_d are positive definite matrices. Hence, e_1 and e_2 exponentially converge to zero, ensuring the tracking of a desired trajectory. ■

Remark 1: *If an integral action with integral constant $K_i = diag(k_{iy}, k_{i\theta}, k_{i\ell})$ is appended to (10), Proposition 1 still holds if the entries of K_i are tuned as $k_{ij} > 0$ and $k_{ij} < k_{pj}k_{dj}$, for $j \in \{y, \theta, \ell\}$.* ◁

B. Stability of the Lateral Dynamics

Assume $\bar{\varrho}(x_1, x_2, v_1) = \varrho(x_1, x_2, v_1)$, substituting $\bar{\varrho}(x_1, x_2, v_1)$ given by (11) in the lateral dynamics of (9) yields

$$\begin{pmatrix} \dot{e}_3 \\ \dot{e}_4 \end{pmatrix} = \overbrace{\begin{pmatrix} 0 & 1 \\ -k_{px} & -k_{dx} \end{pmatrix}}^{A} \begin{pmatrix} e_3 \\ e_4 \end{pmatrix} + \overbrace{\begin{pmatrix} 0 \\ 1 \end{pmatrix}}^{b} \gamma \tag{13}$$

where $e_3 := \bar{x}_{1_1} - x_{1_1}$, $e_4 := \dot{e}_3$, and $\gamma := \varrho(x_1, x_2, v) - \bar{\varrho}(x_1, x_2, v_1)$.

Proposition 2: *If $\gamma \longrightarrow 0$, the virtual control input $\varrho(x_1, x_2, v_1)$ exponentially stabilizes the lateral dynamics.*

Proof: $\gamma \longrightarrow 0 \Leftrightarrow \varrho(x_1, x_2, v) \approx \bar{\varrho}(x_1, x_2, v_1)$. Then, substituting $\bar{\varrho}(x_1, x_2, v_1)$ in the lateral dynamics of (9) results in an autonomous error dynamics with system matrix A given by (13). A is Hurwitzian provided that k_p, $k_d > 0$. As a result, e_3 and e_3 exponentially converge to zero, ensuring the tracking of a desired lateral trajectory. ■

Remark 2: *Intuitively, $\gamma \longrightarrow 0$ can be achieved by tuning the control parameters of the pitch and manipulator dynamics in a way that their dynamics is a time scale faster than the lateral dynamics.* ◁

Proposition 3: *If $\gamma \neq 0$ and $\| \gamma \|_\infty < \sigma < \infty$, $\bar{\varrho}(x_1, x_2, v_1)$ results in bounded - input bounded state (BIBS) stable system. Alternatively stated, the resulting dynamics (13) is Input-State stable (ISS) [13].*

Proof: If $\gamma \neq 0$, substituting $\bar{\varrho}(x_1, x_2, v_1)$ in the lateral dynamics results in a linear error dynamics given by (13), with input γ. Using the well known solution of first order linear system, the requirement on the system's ISS is equivalently translated as, by abuse of notation, the error trajectories ($e = \begin{bmatrix} e_3 & e_4 \end{bmatrix}^T$) fulfilling the following condition [13],

$$| \mathbf{e}(t) | \leq \| e^{At} \| e(0) + (\| b \| \int_0^\infty e^{As} ds) \| \gamma \|_\infty \tag{14}$$

It is trivial to observe that the above inequality always holds because A is Hurwitzian. ■

Remark 3: *Considering the fact that the system has saturated actuator inputs and $\|x_{1_3}\|_\infty < \frac{\pi}{2} \Rightarrow 0 < |\cos(x_{1_3})| < 1$, the assumption that $\| \gamma \|_\infty < \sigma$ is a mild restriction on $x_{2_3}^2$ being bounded.* ◁

C. Stability of the Cascaded System

To show the stability of the two connected systems, we observe the interconnection dynamics. Due to mainly the assumption that $\bar{\varrho}(x_1, x_2, v_1) \approx \varrho(x_1, x_2, v_1)$, the controlled lateral dynamics given by (13) is perturbed by $\tilde{\varrho} = \varrho(x_1, x_2, v_1) - \bar{\varrho}(x_1, x_2, v_1)$. As a result, the lateral error dynamics becomes

$$\begin{pmatrix} \dot{e}_3 \\ \dot{e}_4 \end{pmatrix} = \begin{pmatrix} 0 & 1 \\ -k_{px} & -k_{dx} \end{pmatrix} \begin{pmatrix} e_3 \\ e_4 \end{pmatrix} + \begin{pmatrix} 0 \\ 1 \end{pmatrix} \gamma + \begin{pmatrix} 0 \\ 1 \end{pmatrix} \tilde{\varrho} \tag{15}$$

Based on the growth rate conditions for stability of cascaded systems, provided in [14], and following similar procedures as in [15], it can be shown that e_3 and e_4 are clearly defined and there exists a finite time $t \in \mathbb{R}$ in which $\tilde{\varrho} \longrightarrow 0$. Alternatively stated, the states of the lateral dynamics do not blowup in finite time. Hence, we can deduce that the two system converge.

V. Simulation Results

In this section, simulation results that validate the proposed controller are presented. The system model and control parameters used in the simulation are given in Table I.

A. Tracking Performance and Robustness

In this simulation, it is shown that a desired lateral and vertical trajectories are robustly tracked by the proposed controller in the presence of initial measurement error, random Gaussian measurement noise and parametric uncertainties. Fig. 3 shows the reference and actual states of the planar aerial manipulator. The large tracking error at the beginning is mainly due to initial measurement error but it quickly converges to nearly zero.

TABLE I

MODEL AND CONTROL PARAMETERS IN SI UNITS.

Planar Aerial Manipulator parameters	
$m_u = 1.3$, $m_m = 0.2$	$I_u = 0.15$, $I_m = 0.005$
$c = 0.2$, $h = 0.05$	$g = -9.8$, $\ell \in \boxed{0.2 \quad 0.52}$
$\bar{\mathcal{F}}_1 = \bar{F}_1 = 12$	$\bar{F}_3 = 5$
Control Parameters	
$k_{(px)} = k_{(py)} = 24.5$	$k_{(p\theta)} = 400$, $k_{(p\ell)} = 1000$
$k_{(dx)} = k_{(dy)} = 10$	$k_{(d\theta)} = 210$, $k_{(d\ell)} = 490$
$k_{(ix)} = k_{(iy)} = 8$	$k_{(i\theta)} = k_{(i\ell)} = 100$

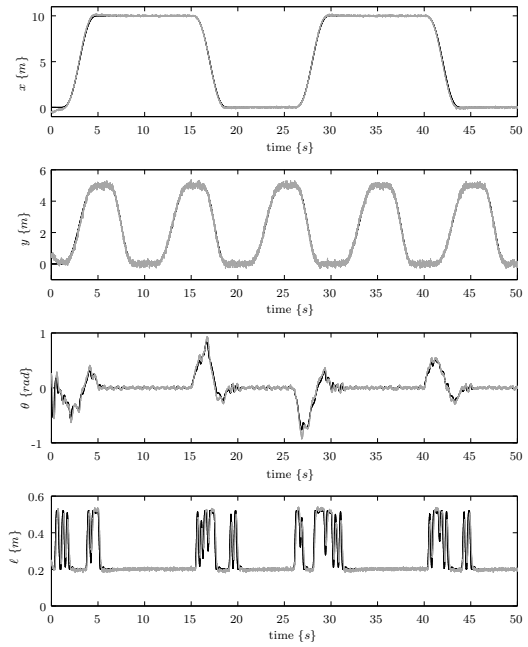

Fig. 3. States of the planar aerial manipulator. The references are indicated by dark lines, whereas the actual states are indicated by gray.

B. Maneuverability Comparison

This simulation compares the achievable maneuverability of the aerial manipulator using three controllers, i.e, the classical PID controller, the proposed controller with the motion of the manipulator constrained at the center $\frac{\bar{\ell}+\underline{\ell}}{2}$, and the controller that exploits the dynamics of the manipulator. Due to the underactuation of the lateral dynamics and its strong coupling with the pitch dynamics, aggressive correction of error in the pitch trajectory is fundamental for the control of the lateral dynamics. Thus, the comparison is made by particularly observing the pitch dynamics.

Fig. 4 shows the pitch tracking performance of the three controllers. Clearly, the controllers designed based on the unified dynamics of the aerial manipulator outperform the PID controller in the entire trajectory. However, in the second half of the trajectory where the maneuver requires more input torque than that can be delivered by the thrust alone, the performance of the proposed controller that exploits the dynamics of the manipulator is better than the rest.

VI. EXPERIMENTS

In this section, the experimental setup and results are presented. The aerial manipulator used for experiment is mainly composed of a delta manipulator [6], on which a gripper is mounted, and a pelican quadrotor [16], see Fig 5. The manipulator was designed by the University of Twente as a part of the AIRobots project [17] for aerial inspection by contact. It has three actuated DOFs in the Cartesian space and is equipped with a joint space position controller.

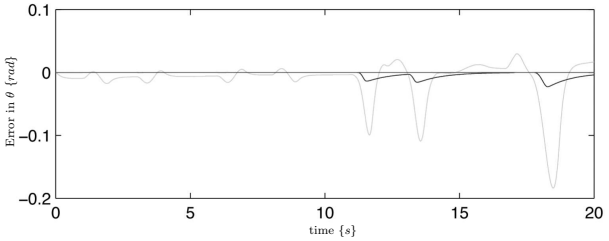

Fig. 4. Comparison of pitch (θ) tracking capabilities of different controllers; the commonly used PID controller (light gray), the proposed controller with the manipulator constrained at $\frac{\bar{\ell}+\underline{\ell}}{2}$ (dark), and the controller that exploits the dynamics of the manipulator (dark gray).

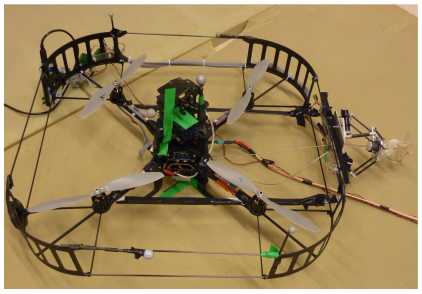

Fig. 5. The aerial manipulator used for experimentation.

During the experiments, the absolute pose of the UAV is provided by external tracking system. The position of the end-effector, on which the mass is assumed to be concentrated at, is estimated based on joint angles obtained from the motor encoders. The control and communication software structure is implemented in ROS and Simulink.

Fig. 6 shows result from the trajectory tracking experiment for two different controllers in the presence of initial measurement error and system parameter uncertainties. The implemented controller are a PID controller with compensating mass (appended to compensate for the static bias torque due to the action of gravity on mass of the manipulator) and the proposed controller that exploits the dynamics of the manipulator. Fig. 6 shows that the proposed controller results in a better tracking than the PID controller with compensating mass. The slow response and poor tracking performance of the PID controller is mainly attributed to the higher inertia of and larger gravitational effect on the aerial manipulator than the UAV alone, for which the control parameters has been originally tuned.

VII. CONCLUSION

In this paper, we have proposed a new control architecture that is based on the unified dynamics of an aerial manipulator and exploits the additional dynamic disturbance of the manipulation system for free-flight control of the UAV. A clear comparison between the state-of-the-art and the proposed controller is also presented. From tracking performance and maneuverability point of view, the proposed controller has shown superiority over the classical UAV controllers.

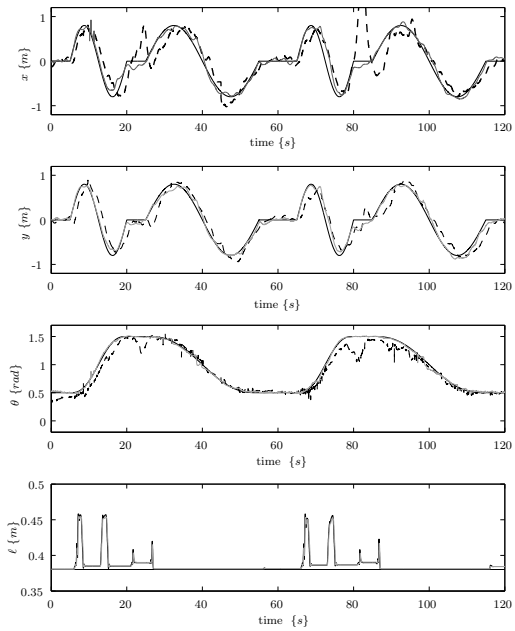

Fig. 6. Comparison of the tracking capabilities of the proposed controller (red) and the PID controller with compensating mass (green).

The proposed architecture relaxes the light-weight requirement and placement restrictions, which as a consequence, extends the application spectrum that aerial manipulators can be considered. It also opens opportunities for using manipulators of different mechanical configuration and dynamic property. Furthermore, this work can be used as a basis for exploiting aerially transported loads and external interaction forces to improve the tracking or other secondary task performance of UAVs.

APPENDIX

A. Model matrices and vectors

$$M(x_1) = \begin{bmatrix} m_{11} & m_{12} & m_{13} & m_{14} \\ m_{21} & m_{22} & m_{23} & m_{24} \\ m_{31} & m_{32} & m_{33} & m_{34} \\ m_{41} & m_{42} & m_{43} & m_{44} \end{bmatrix}$$

where

$m_{11} = m_{22} = m_u + m_m$; $m_{12} = m_{21} = 0$
$m_{13} = m_{31} = -m_m(\ell \sin(\theta) + h\cos(\theta))$
$m_{14} = m_{41} = m_m \cos(\theta)$; $m_{24} = m_{42} = m_m \sin(\theta)$
$m_{23} = m_{32} = m_m(\ell \cos(\theta) - h\sin(\theta))$
$m_{34} = m_{43} = -m_m h$
$m_{33} = I_u + I_m + m_m(\ell^2 + h^2)$; $m_{44} = m_m$

$$C(x_1, x_2) = \begin{bmatrix} c_{11} & c_{12} & c_{13} & c_{14} \\ c_{21} & c_{22} & c_{23} & c_{24} \\ c_{31} & c_{32} & c_{33} & c_{34} \\ c_{41} & c_{42} & c_{43} & c_{44} \end{bmatrix}$$

where

$c_{13} = m_m\{2\dot{\ell}\sin(\theta) + (\ell\cos(\theta) - h\sin(\theta))\dot{\theta}\}$
$c_{23} = m_m\{2\dot{\ell}\cos(\theta) - (\ell\sin(\theta) + h\cos(\theta))\dot{\theta}\}$
$c_{33} = 2m_m\ell\dot{\ell}$
$c_{41} = -m_m\ell\dot{\theta}$, and the rest of the entries are zero.

$D = diag(d_x, d_y, d_\theta, d_\ell)$

$$G(x_1) = -\begin{bmatrix} 0 \\ (m_u + m_m)g \\ (\ell\cos(\theta) - h\sin(\theta))m_m g \\ m_m g \sin(\theta) \end{bmatrix}$$

$$B(x_1) = \begin{bmatrix} -\sin(\theta) & -\sin(\theta) & 0 \\ \cos(\theta) & \cos(\theta) & 0 \\ c & -c & 0 \\ 0 & 0 & 1 \end{bmatrix}$$

$$\varrho(x_1, x_2, v) = -\{v_1 - g + \tfrac{d_y}{m_u+m_m}\dot{x}_{1_2}\}\tan(x_{1_3}) - \tfrac{1}{m_u+m_m}\{d_x\dot{x}_{1_1} + \tfrac{m_m}{\cos(x_{1_3})}(v_3 - hv_2 - \ell\dot{x}_{1_3}^2)\}$$

$$\varrho(x_1, x_2, v_1) = -\{v_1 - g + \tfrac{d_y}{m_u+m_m}\dot{x}_{1_2}\}\tan(x_{1_3}) - \tfrac{d_x}{m_u+m_m}\dot{x}_{1_1}$$

REFERENCES

[1] M. Fumagalli, R. Naldi, A. Macchelli, R. Carloni, S. Stramigioli, and L. Marconi, "Modeling and control of a flying robot for contact inspection," in *Proceedings of the IEEE International Conference on Intelligent Robots and Systems*, 2012.

[2] P. Pounds, R. Mahony, and P. Corke, "Modelling and Control of a Quad-Rotor Robot," in *Proceedings of the Australasian Conference on Robotics and Automation*, 2006.

[3] M. Orsag, C. Korpela, and P. Oh, "Modeling and control of mm-uav: mobile manipulating unmanned aerial vehicle," *Journal of Intelligent and Robotic Systems*, pp. 227–240, 2013.

[4] I. Palunko, P. Cruz, and R. Fierro, "Agile Load Transportation: Safe and Efficient Load Manipulation with Aerial Robots," *IEEE Robotic and Automation Magazine*, vol. 19, no. 3, pp. 69–79, 2012.

[5] D. Mellinger, M. Shomin, and V. Kumar, "Control of Quadrotors for Robust Perching and Landing," in *International Powered Lift Conference*, 2006.

[6] A. Keemink, M. Fumagalli, S. Stramigioli, and R. Carloni, "Mechanical design of manipulation system for unmanned aerial vehicle," in *Proceedings of the IEEE International Conference on Robotics and Automation*, 2012.

[7] I. Maza, K. Kondak, M. Bernand, and A. Ollero, "Multi-UAV Cooperation and Control for Load Transportation and Deployment," *Journal of Intelligent and Robotic Systems*, vol. 57, no. 1, pp. 417–449, 2010.

[8] J. Levine, *Analysis and Control of Nonlinear Systems*, vol. 115. Springer-Verlag Berlin Heidelberg, 2009.

[9] D. Mellinger and V. Kumar, "Minimum snap trajectory generation and control for quadrotors," in *Proceedings of the IEEE International Conference on Robotics and Automation*, 2011.

[10] H. Nijmeijer and A. van der Schaft, *Nonlinear dynamical control systems*. Springer-Verlag New York, Inc., 1990.

[11] R. Naldi, L. Gentili, L. Marconi, and A. Sala, "Design and experimental validation of a nonlinear control law for ducted fan miniature aerial vehicle," *Control Engineering Practice*, vol. 18, no. 7, pp. 677–836, 2010.

[12] A. Y. Mersha, R. Carloni, and S. Stramigioli, "Modeling and control of underactuated aerial vehicles," in *Proceedings of the IEEE International Conference on Robotics and Automation*, 2011.

[13] A. A. Agrachev, A. S. Morse, E. D. Sontag, H. J. Sussmann, and V. I. Utkin, *Nonlinear and Optimal Control Theory*. Springer-Verlag, Berlin Heidelberg, 2008.

[14] E. Panteley and A. Loria, "Growth rate conditions for stability of cascaded time-varying systems," *Automatica*, vol. 37, no. 3, pp. 453–460, 2001.

[15] J. Pflimlin, T. Hamel, P. Soueres, and R. Mahony, "A hierarchical control strategy for the autonomous navigation of a ducted fan flying robot," in *Proceedings of the IEEE International Conference on Robotics and Automation*, 2006.

[16] Ascending Technologies GmbH (AscTec). http://www.asctec.de.

[17] L. Marconi, L. Basile, G. Caprari, R. Carloni, P. Chiacchio, C. Huerzeler, V. Lippiello, R. Naldi, N. Janosch, B. Siciliano, S. Stramigioli, and E. Zwicker, "Aerial service robotics: the airobots perspective," in *Proceedings of the IEEE International Conference on Applied Robotics for the Power Industry*, 2012.